

Phase transitions of MnP for a field parallel to the hard-magnetization direction: A possible new Lifshitz point

Y. Shapira

*Francis Bitter National Magnet Laboratory, Massachusetts Institute of Technology,
Cambridge, Massachusetts 02139*

N. F. Oliveira, Jr. and C. C. Becerra

Instituto de Fisica, Universidade de São Paulo, Caixa Postal 20516, São Paulo 05508, Brazil

S. Foner

*Francis Bitter National Magnet Laboratory and the Department of Physics,
Massachusetts Institute of Technology, Cambridge, Massachusetts 02139*

(Received 19 August 1983)

The phase transitions and phase diagram of MnP in the presence of a magnetic field \vec{H} parallel to the a axis were investigated with the use of differential susceptibility, magnetostriction, thermal expansion, magnetization, and ultrasonic measurements. Three ordered phases were observed. One is the ferromagnetic phase. The other two are tentatively identified as fan and cone phases. The disordered (paramagnetic) phase, and the ferromagnetic and fan phases, meet at the paramagnetic-ferromagnetic-fan (PFF) triple point, located at $T_i = 121$ K and $H = 51$ kOe. The phase diagram near this triple point has a striking similarity to that near the corresponding point in the phase diagram for $\vec{H} \parallel b$. The fan-paramagnetic and ferromagnetic-paramagnetic transitions are of second order, but the ferromagnetic-fan transitions are of first order. The qualitative features of the phase diagram near the PFF triple point and the crossover exponent $\phi = 0.64 \pm 0.02$ are consistent with those expected for a Lifshitz point. The cone, ferromagnetic, and fan phases meet at another triple point, located at $T \simeq 60$ K and $H = 41$ kOe. The ferromagnetic-cone transitions are of first order. The cone-fan transitions are weakly first order at high temperatures, but there is an uncertainty concerning the order of these transitions at low temperatures. An anomaly in the magnetostriction and differential susceptibility was observed at low magnetic fields (several kOe). This anomaly is attributed to imperfections of the crystals.

I. INTRODUCTION

Manganese phosphide exhibits several magnetic phases and a variety of phase transitions. The structures of the magnetic phases, and the phase transitions, have been the subjects of many experimental investigations in the last two decades.¹ The interest in MnP increased considerably in the last three years after strong evidence for the existence of a Lifshitz point (LP) in this material was found.²⁻⁷ In the present paper we report on measurements of the phase transitions and the phase diagram when the magnetic field \vec{H} is parallel to the hard magnetization direction. Transitions for this field direction were not studied previously. The two main points of the present work are (1) it appears that a LP also exists when \vec{H} is parallel to the hard-magnetization direction, and (2) a new phase boundary is observed and is interpreted as the line separating a cone phase from a fan phase. A preliminary report was published previously.⁸

MnP has an orthorhombic structure. Here we make the usual (but not universal) choice for the axes of the orthorhombic unit cell, namely, $a > b > c$. The available information concerning the magnetic properties of MnP was summarized in recent publications by our group^{3,7}

and in two earlier papers.^{9,10} Below we repeat only the main relevant facts.

At zero magnetic field, MnP exhibits two magnetically ordered phases: ferromagnetic and screw. When the material is cooled from high temperatures, it first becomes ferromagnetic at the Curie temperature $T_C = 291$ K, but on further cooling through $T_\alpha \simeq 46$ K, a screw phase is formed. The paramagnetic to ferromagnetic (para-ferro) transition at T_C is of second order, whereas the ferro-screw transition at T_α is of first order. The value of T_α depends slightly on sample purity.¹¹ In the ferro phase the magnetic moment is along the c axis, which is the easy direction. The b and a directions are the medium- and hard-magnetization directions, respectively. The magnetic structure of the screw phase is that of a spiral, with a propagation vector \vec{q} along a , and with the moments rotating in the c - b plane (easy-medium plane). The period is approximately 9 lattice spacings.¹²

The magnetic behavior in the presence of a magnetic field \vec{H} along the c axis (easy-magnetization axis) was first measured by Huber and Ridgley.¹³ The main feature is a field-induced first-order transition from the screw phase to the ferro phase. The magnetic field at the transition decreases continuously from approximately 2.3 kOe at

helium temperatures to zero at T_a .

The phase diagram when \vec{H} is parallel to the b axis was measured by Komatsubara *et al.*,⁹ and more carefully by our group.^{2,3} Figure 1, taken from Ref. 3, shows the global phase diagram for this field direction. An important feature is the existence of a fan phase, which is a modulated phase with a propagation vector \vec{q} parallel to a .¹⁴ The moments in the fan phase are in the b - c plane, and they oscillate about the b direction (which is also the direction of \vec{H}). The screw-fan, screw-ferro, and ferro-fan transitions are all of first order, but the ferro-para and fan-para transitions are of second order. Much of the recent interest in MnP centers on the point where the para, ferro, and fan phases meet. The available evidence²⁻⁷ is that this point is a LP. The concept of the LP was introduced theoretically by Hornreich, Luban, and Shtrikman.¹⁵ The extensive theoretical work concerning this multicritical point was reviewed by Hornreich.¹⁶ The data on MnP provide the strongest evidence to date for the existence of a LP in a real material.

A detailed microscopic theory for the magnetic behavior of MnP is not available at present. A model which is often used was introduced by Hiyamizu and Nagamiya.¹⁰ In this model the modulated phases (screw and fan) arise from a competition between effective ferromagnetic and antiferromagnetic exchange interactions. There is experimental evidence that the strength of the antiferromagnetic interaction decreases slightly as the temperature T is raised, and that this decrease is sufficient to make the ferro phase the stable ordered phase at high temperatures.¹⁷ This phenomenological interpretation of the magnetic behavior of MnP was also used to explain the existence of a LP in the configuration $\vec{H}||b$.^{3,5-7} The simplest theoretical models for the LP are the R - S and anisotropic next-nearest-neighbor Ising models (ANNNI).^{18,19} In these models there are two competing exchange interactions, with constants J_1 and J_2 . A measure of the competition is the ratio $\kappa = J_2/J_1$. The LP occurs when κ passes through the special value κ_L . In the mean-field theory $\kappa_L = -0.25$. Treatments which go beyond mean-field theory lead to slightly different values for κ_L .¹⁸ The available experimental data for the effective exchange constants in MnP (Ref. 17) indicate that the pa-

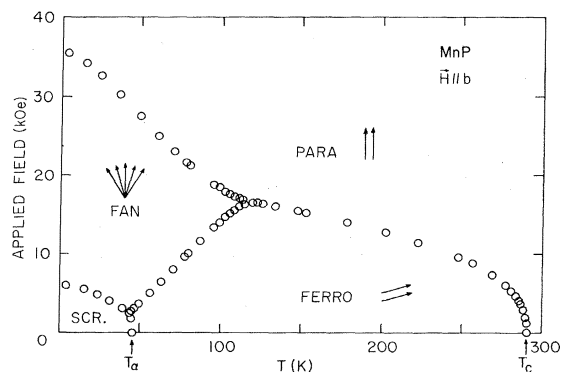


FIG. 1. Global phase diagram of MnP with the applied magnetic field \vec{H}_0 parallel to the b direction (after Ref. 3).

rameter κ (or its generalization to more than two exchange constants) is indeed close to κ_L . Moreover, κ changes slowly with T and it passes through -0.25 at a temperature which is close to that of the para-ferro-fan triple point.

This paper is arranged as follows. In Sec. II we describe the experimental techniques. In Sec. III the global phase diagram for the configuration $\vec{H}||a$ is presented and the gross features of this diagram are interpreted. In Sec. IV detailed data for the boundary between the ferro phase and the para phase are presented. The fan-ferro and fan-para boundaries are described in Sec. V. The new multicritical point (believed to be a LP) is discussed in Sec. VI. Section VII is devoted to the boundaries which surround the cone phase. In Sec. VIII we describe some anomalies which were observed at low H and which are attributed to imperfections of the samples. Suggestions for further studies are outlined in Sec. IX.

II. EXPERIMENTAL TECHNIQUES

A. Samples

Three samples were used in the present work. Two of these, which will be called A1 and A2, were also used in the earlier work by our group.^{2,3} They were cut from a crystal which was grown at the Lincoln Laboratory, Massachusetts Institute of Technology (MIT) more than a decade ago. The third sample, called sample B, was obtained from Dr. B. Golding of the Bell Telephone Laboratories. X-ray examinations showed that the samples were single crystals. However, as discussed in Sec. VIII, there is some evidence from magnetic measurements that each of the samples contained small regions which were misoriented relative to the bulk of the sample. The volume fraction occupied by these misoriented regions was $\sim 1\%$ for samples A1 and A2, and smaller for sample B. All samples were rectangular parallelepipeds, with faces parallel to the a , b , and c planes. The linear dimensions of the samples were as follows. For sample A1, $l_a = 4.0$ mm, $l_b = 3.0$ mm, and $l_c = 0.5$ mm. For sample A2, $l_a = 0.97$ mm, $l_b = 2.67$ mm, and $l_c = 0.84$ mm. For sample B, $l_a = 5.7$ mm, $l_b = 10.3$ mm, and $l_c = 7.0$ mm.

The experiments reported here were conducted in several stages. In the first, the global phase diagram for $\vec{H}||a$ was determined using sample A2. Later, more detailed measurements of the phase boundaries were made on samples A2 and B. In the final stage, very detailed and accurate data were taken for the most interesting regions of the phase diagram. This final stage was carried out using sample A1, which had the most favorable shape (smallest demagnetization effects).

B. Differential susceptibility

The differential susceptibility $\partial M / \partial H_0$, where M is the magnetization, was measured using ac modulation techniques. The modulation field was parallel to the applied dc field \vec{H}_0 . The susceptibility data were taken in two different laboratories using somewhat different arrangements. In both arrangements there was a primary coil which produced the modulation field, and two pickup

coils wound in opposition which served as the secondary. The sample was placed at the center of one of the pickup coils. In the arrangement at MIT the imbalance signal from the secondary was detected by a lock-in amplifier, and was measured as a function of H_0 at a constant temperature T . The phase of the lock-in amplifier was set to detect the in-phase component of the signal, corresponding to the real part of the susceptibility $\chi = \chi' - i\chi''$. Frequencies of 70–200 Hz and a modulation amplitude of 10 Oe were used with this setup. The temperature control was similar to that described in Sec. III C of Ref. 3, except that the copper cans were replaced by brass cans. Temperatures were measured with a platinum thermometer which was read at $H_0 = 0$ before and after each trace, and also during the trace. The readings in the presence of a field were corrected for the magnetoresistance of the thermometer. The accuracy of the temperature measurements with this setup was 0.2 K above 50 K, 0.4 K near 40 K, and 2 K near 25 K.

At the University of São Paulo the susceptibility was measured with a mutual inductance bridge, similar to that described by Maxwell.²⁰ Frequencies between 20 and 2000 Hz, and a modulation amplitude of order 1 Oe, were used. The imbalance signal from the bridge was measured using a two-phase lock-in amplifier. When the lock-in amplifier was properly tuned, it gave both the in-phase component (χ') and quadrature component (χ'') of the susceptibility. The susceptibility was measured as a function of H_0 at a constant T . The temperature-control system was similar to that described in Sec. III B 1 of Ref. 3. The only difference was that the Allen-Bradley carbon resistor used in the feedback loop which controlled the temperature was moved from the center of the magnet to a region of low fields. Temperatures between 70 and 150 K were measured to an accuracy of 0.05 K using a platinum thermometer. (The magnetoresistance of this thermometer was measured, and was included in the data analysis.) Temperatures between 4 and 70 K were measured using a carbon-resistance thermometer, or a platinum thermometer, or both. The accuracy in this temperature range was always better than 1 K.

C. Magnetostriction, magnetization, and ultrasonic attenuation

Magnetostriction (MS) and thermal-expansion (TE) measurements were made using the system described in Ref. 3. All the MS measurements were in the longitudinal configuration. That is, the variation of the sample's length l along the a direction (parallel to \vec{H}_0) was measured as a function of H_0 at a constant T . The temperature in the TE and MS measurements was determined to an accuracy of better than 0.1 K.

Magnetization measurements were performed using a vibrating-sample magnetometer. Data were taken only at 4.2 and 77 K with the sample immersed in liquid helium and liquid nitrogen, respectively.

The ultrasonic attenuation measurements were made only on sample B. (The other two samples were rather small for ultrasonic work.) A pulse-echo technique was used. The longitudinal sound waves were produced and

detected by the same X -cut quartz transducer. The system for temperature control and measurement was identical to the one used in the MS measurements.

D. Magnetic fields and demagnetization correction

Magnetic fields were produced by Nb-Ti superconducting magnets. The applied magnetic field was known to an accuracy of better than 0.25%.

In magnetic materials it is necessary to distinguish between the applied magnetic field \vec{H}_0 and the internal magnetic field \vec{H} . The difference between the two fields is caused by the demagnetization of the sample. This subject is reviewed in Ref. 3. For an ellipsoidal sample, one may correct for the demagnetization by using the relation

$$H = H_0 - NM, \quad (1)$$

where N is the demagnetizing factor. When the sample is not ellipsoidal the situation is more complicated. However, if the demagnetization correction is small, one can still obtain a fairly accurate estimate for H by using Eq. (1) and an effective demagnetizing factor which is estimated from the shape of the sample. This procedure is reasonably accurate for obtaining the internal fields at the transitions of MnP in the configuration $\vec{H} \parallel a$, because M/H is between 0.6% and 1.3%.

In presenting our data we shall always use the applied field H_0 rather than the internal field H . Estimates for the ratio H/H_0 will be given in several places. They are based on the estimates $N_a \simeq 1$ for sample A1 with $\vec{H} \parallel a$, and $N_a \simeq 5$ for both samples A2 and B (see Ref. 21). The errors in the estimates for H/H_0 are expected to be smaller than 1% for sample A1, and smaller than 2% for the other two samples.

E. Field alignment

Accurate alignment of the magnetic field is very important in measurements of the phase diagram for $\vec{H} \parallel a$. The phase boundaries separating the disordered (paramagnetic) phase from the ordered phases are particularly sensitive to field misalignment. Some of the reasons for this sensitivity were discussed in our earlier work on the phase transitions for \vec{H} nearly parallel to the b axis (see Sec. VI of Ref. 3). There we focused on the effects produced by a nonzero c component of \vec{H} . Similar effects due to a small nonzero c component should also occur when \vec{H} is nearly parallel to a . In addition, because of the anisotropy in the a - b plane, the transition fields are influenced by a misalignment of \vec{H} in this plane.

In order to align the magnetic field accurately, the transition between the paramagnetic and fan phases (discussed later) was monitored at a fixed temperature near 80 K. Accurate field alignment led to the sharpest transition and highest transition field. In the experiments on samples A2 and B the direction of \vec{H} relative to the sample was changed by tipping the sample holder. The alignment achieved with this method was estimated to be better than 0.5°. A more refined method was used in the experiments

on sample A1. Here, the sample's orientation was fixed, but the direction of \vec{H} was changed by tipping the superconducting magnet. The tipping mechanism is described in Ref. 22. An alignment which was better than 0.1° was achieved in these experiments.

III. GLOBAL PHASE DIAGRAM

The purpose of this section is to give an overview of the phase diagram for $\vec{H}_0 \parallel a$. A more detailed discussion of the various phase transitions and phase boundaries is given in subsequent sections.

The global phase diagram for $\vec{H}_0 \parallel a$ was determined from susceptibility measurements and from TE and MS data, all carried out on sample A2. The results are shown in Fig. 2. There are three ordered phases in addition to the disordered (paramagnetic) phase. Among the three ordered phases only the ferro phase can be identified with certainty. This identification is based on earlier results which established that the magnetic order at zero field and for $T_\alpha < T < T_C$ is ferromagnetic.

The magnetic structures of the other two ordered phases have not been determined as yet by neutron diffraction. Nevertheless, we feel reasonably confident that the magnetic structure of these two phases are those of a cone and a fan. The reasoning behind these tentative identifications is the following. It is known that at zero field and for $T < T_\alpha$ the magnetic structure is that of spiral with the moments rotating in the plane perpendicular to the a axis. When a weak magnetic field is applied along a the moments are expected to tip toward the direction of \vec{H} , so that the structure becomes that of a cone, with its axis and propagation vector \vec{q} both parallel to a . The magnitude of q may vary with H . The identification of the fan phase is based on the striking similarity between Fig. 2 for $\vec{H}_0 \parallel a$ and Fig. 1 for $\vec{H}_0 \parallel b$. We expect that the fan phase for $\vec{H}_0 \parallel a$ has the following structure: (1) The propagation vector \vec{q} is parallel to a , and (2) the moments oscillate about the a axis (which is also the direction of \vec{H}), remaining always in the a - c plane (which is the plane containing \vec{H} and the easy axis).

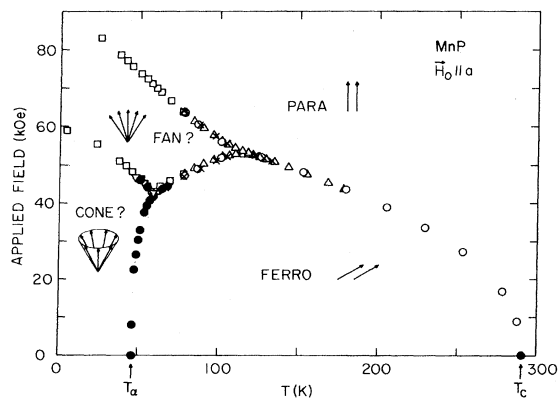


FIG. 2. Global phase diagram for \vec{H}_0 parallel to the a direction. Data are for sample A2.

The magnetic structures of MnP in the presence of a field along a have not been calculated thus far. However, there do exist calculations by Kitano and Nagamiya for somewhat similar situations.²³ Our preceding identifications of the cone and fan phases are in line with these available calculations.

Figure 3 shows our picture for the evolution of the magnetic structure of MnP for $T < T_\alpha$. This picture is based on results of Kitano and Nagamiya for a similar situation. It shows the sequence spiral \rightarrow cone \rightarrow fan \rightarrow para for a monotonically increasing magnetic field. Consider the cone phase. From the work of Kitano and Nagamiya we expect that the cone is an elliptical cone and not a circular cone. That is, the amplitude m_c of the oscillating c component of the magnetization (along the easy direction) is larger than the amplitude m_b of the oscillating b component (along the medium anisotropy direction).²⁴ Both amplitudes decrease with increasing H , but m_b decreases faster than m_c . In the fan phase, $m_b = 0$, but $m_c \neq 0$. In the para phase, $m_c = m_b = 0$, i.e., the magnetization is uniform and is parallel to a .

The cone-to-fan transition occurs when m_b becomes equal to zero. In principle, the transition may be either of first order or second order. That is, m_b may jump from a finite value in the cone phase to zero in the fan phase, or it may go to zero continuously. The case of a second-order transition was considered by Kitano and Nagamiya. Here, we include the possibility of a first-order transition because our data for temperatures above approximately 15 K suggest that at these temperatures the cone-fan transition is weakly first order. For temperatures below 15 K or so, our data indicate that the transition is either of second order or is very weakly first order. This will be discussed in Sec. VII.

The fan-para transition is observed to be of second order. This transition occurs because in the fan phase the

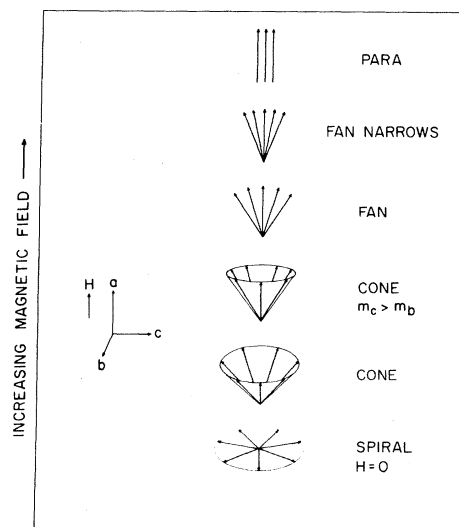


FIG. 3. Schematic of the expected evolution of the magnetic structure with increasing magnetic field H for a temperature T below T_α . Field \vec{H} is parallel to a . Magnetic structures are viewed from a point which is in the a - b plane, and above the b axis.

amplitude m_c of the oscillating c component of the magnetization decreases with increasing H , so that, ultimately, a transition to a para phase with $m_c = 0$ takes place.

At temperatures above approximately 121 K, a transition from the ferro phase to the para phase takes place. This transition is observed to be of second order. The transition occurs because in the ferro phase the moments tip toward \vec{H} as H increases, so that ultimately the moments become parallel to \vec{H} . The ferro \rightarrow para transition corresponds, therefore, to the vanishing of the uniform c component of the magnetization of the ferro phase. This magnetization component is the order parameter for the transition. The ferro-para transition is expected to be Ising-like. The ferro-fan and ferro-cone transitions are observed to be of first order.

In concluding this discussion of the overall phase diagram we wish to emphasize again that our identifications of the cone and fan phases are tentative because no neutron-diffraction data for these phases are available. Thus although we shall continue to use the names "cone" and "fan," some uncertainty regarding the proper identification of these two phases still remains.

IV. FERRO-PARA PHASE BOUNDARY

The ferro-para phase boundary was determined from measurements of $\partial M / \partial H_0$ for sample A2 and from measurements of the ultrasonic attenuation in sample B. In the latter case, 23- and 75-MHz longitudinal sound waves with a propagation vector along a were used. In both types of measurements the ferro-para transition appeared as a λ peak of the signal versus H_0 at a constant T . The λ peak became less pronounced as T decreased. This is illustrated by the lowest four curves in Fig. 4. In the case of the susceptibility data, $\partial M / \partial H_0$ vs H_0 , the transition field was chosen at the intersection of the two tangents drawn at the inflection points on both sides of the peak (see inset in Fig. 4). This choice was motivated by the fact that the susceptibility peaks at the lowest temperatures were small and slightly rounded. On the other hand, the ultrasonic attenuation peaks were always quite sharp and the transition field was chosen at the maximum of the attenuation.

The Curie temperature of sample B was determined from the λ peak of the ultrasonic attenuation versus T at $H_0 = 0$. This gave $T_C = 290.7 \pm 0.2$ K. The Curie temperature of sample A2 was not measured, but earlier data on a sample from the same single crystal gave $T_C = 291$ K.³

Figure 5 shows the portion of the ferro-para phase boundary above 200 K. The applied magnetic field at the transition will be designated as $H_{0\lambda}$. The demagnetization correction for the results in Fig. 5 is estimated as follows. The susceptibility χ_a for $\vec{H} \parallel a$ is 13×10^{-3} emu/cm³ near T_C ,²⁵ and 8×10^{-3} emu/cm³ at 100 K.¹³ We assume a smooth variation of χ_a between these two temperatures, and use Eq. (1) and the estimate $N_a \approx 5$ for both samples A2 and B. The ratio $H_\lambda / H_{0\lambda}$ between the internal and applied fields at the transition then varies between 0.94 near T_C and 0.95 near 200 K.

The existence of a H -induced second-order transition

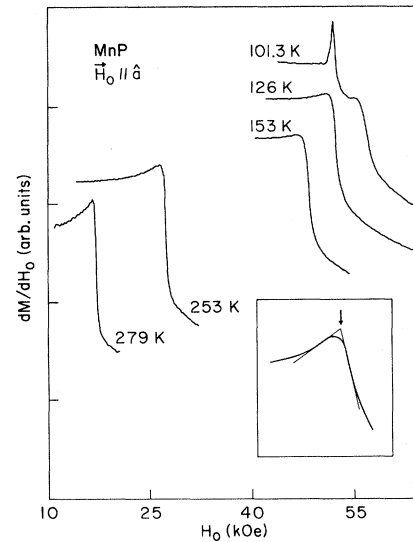


FIG. 4. Traces of the differential susceptibility dM/dH_0 of sample A2 as a function of H_0 . Various traces were displaced relative to each other in the vertical direction. Lowest four traces show the ferro-para transition. Top trace shows the ferro-fan transition (spike) and the fan-para transition (shoulder). Inset shows the manner in which the transition field was chosen when the transition was of second order.

from the ferro phase to the para phase is expected from the theory for anisotropic ferromagnets.^{5,26,27} Such a transition was studied earlier in $\text{NiZrF}_6 \cdot 6\text{H}_2\text{O}$ (Ref. 28). The expected critical behavior and the scaling axes for the ferro-para transition were discussed previously for the configuration $\vec{H} \parallel b$.³ The present case, for $\vec{H} \parallel a$, is completely analogous. A comparison between Figs. 1 and 2 shows that at a given T the ferro-para transition for $\vec{H} \parallel a$ occurs at a higher field than for $\vec{H} \parallel b$. This is expected from the different anisotropies associated with these directions.

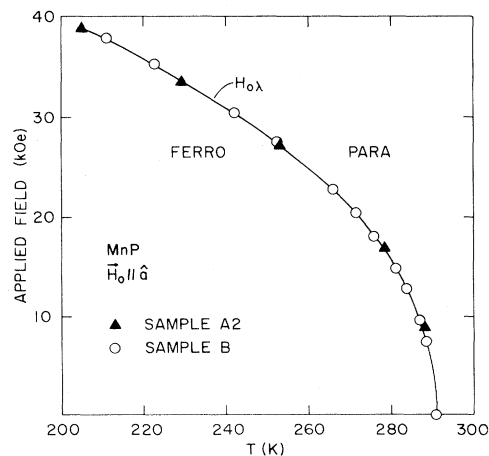


FIG. 5. High-temperature portion of the ferro-para phase boundary as determined from ac susceptibility data on sample A2 and ultrasonic attenuation data on sample B.

V. FERRO-FAN AND FAN-PARA BOUNDARIES

The ferro-fan and fan-para phase boundaries were initially determined from measurements on samples A2 and B with the magnetic field aligned to within 0.5° from the a axis. Later, a more careful investigation was carried out using sample A1 with the field aligned to better than 0.1° . The demagnetizing factor for sample A1 ($N_a \simeq 1$) was also more favorable than for the other two samples ($N_a \simeq 5$). We begin by describing the results for samples A2 and B.

Phase transitions in sample A2 were investigated using differential susceptibility and MS measurements. Transitions in sample B were studied only by the MS technique. An example of the behavior of the susceptibility near the ferro-fan and fan-para transitions is the top curve in Fig. 4 for 101.3 K. The ferro-fan transition is marked by a sharp spike in $\partial M/\partial H_0$. The fan-para transition is associated with a "shoulder" in the susceptibility curve. The transition field was chosen in the manner indicated by the inset in Fig. 4.

The MS measurements in samples A2 and B gave very similar results. These are illustrated by the data in Fig. 6(a). Here, Δl is the change in the length of the sample along the a direction. The ferro-fan transition (which is of first order) is associated with an abrupt jump δl in the length l . For the example shown in Fig. 6(a) the magnitude of the abrupt jump is $\delta l/l \simeq 8 \times 10^{-6}$. The fan-para transition is accompanied by an anomaly in the slope of the MS curve.

To obtain the transition fields from the MS data it is preferable to focus on the derivative $\partial l/\partial H_0$ rather than on the raw data for l vs H_0 . This is discussed in Ref. 3. A first-order transition is marked by a positive or a negative spike in $\partial l/\partial H_0$. This corresponds to an abrupt change in l . A second-order transition is accompanied by

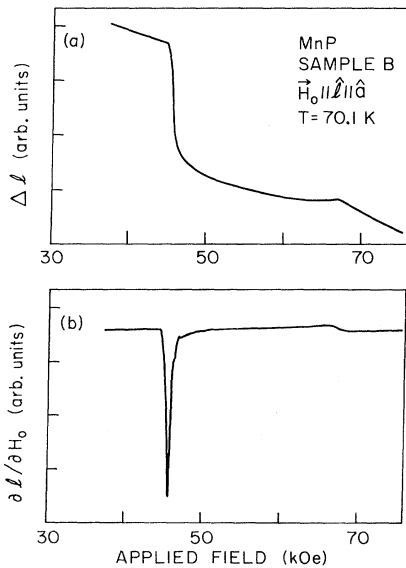


FIG. 6. MS and differential MS at 70.1 K. (a) Trace of the longitudinal MS. Sample's length l along the a direction ($\hat{l} \parallel \hat{a}$) is measured with \vec{H}_0 also along the a direction. Δl is the change of l . (b) The derivative $\partial l/\partial H_0$ obtained by a numerical differentiation on the data in (a).

a λ anomaly in $\partial l/\partial H_0$. In some cases the λ anomaly resembles a step. This occurs when the critical fluctuations are weak, or when the internal magnetic field is not uniform (which broadens the λ anomaly).

Figure 6(b) shows the derivative $\partial l/\partial H_0$ obtained by a numerical differentiation of the data in Fig. 6(a). The negative spike at the ferro-fan transition is clear. The fan-para transition appears to be associated with a small step in $\partial l/\partial H_0$. However, an expanded view of the variation of $\partial l/\partial H_0$ near the fan-para transition shows that what appears to be a small step in Fig. 6(b) is actually a λ anomaly. This is shown in Fig. 7. The transition field was chosen in the manner indicated in the inset of Fig. 4.

The ferro-fan and fan-para transitions on sample A2 were also investigated by magnetization measurements, but only at 77 K. The results are shown in Fig. 8. As this trace shows, the ferro-fan transition at 47 kOe is accompanied by a sharp, but small, change of the magnetization M . The fan-para transition at 64 kOe is accompanied by an anomaly in the slope of the magnetization curve. These results are consistent with the susceptibility data.

The high- T portions of the phase boundaries which surround the fan phase are shown in Fig. 9. These data are for sample A2. The results for sample B are in good agreement with those in Fig. 9. The applied magnetic fields at the ferro-fan and fan-para transitions will be designated as H_{01} and $H_{0\lambda}^*$, respectively. The demagnetization correction for the data in Fig. 9 was estimated from the susceptibility data in Ref. 13 using $N_a \simeq 5$. The result is that the internal fields at the transitions, H_1 and H_λ^* , are 4% lower than the corresponding applied fields H_{01} and $H_{0\lambda}^*$.

We now turn to the more refined measurements which were carried out on sample A1. Examples of susceptibility data on this sample are shown in Figs. 10 and 11. One difference between these data and those taken on sample A2 (see the top curve in Fig. 4) is that the fan-para transition is accompanied by a clear λ peak in $\partial M/\partial H_0$. This is attributed to the more favorable shape of sample A1, which led to a more uniform internal magnetic field H , and possibly also to the better field alignment. The ferro-

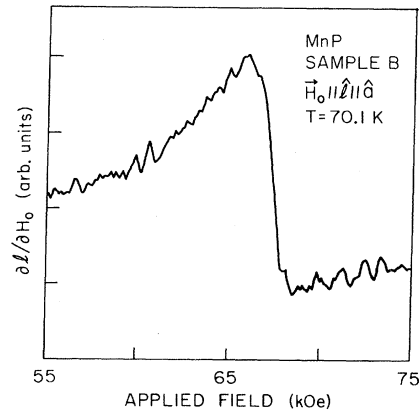


FIG. 7. Expanded view of that portion of Fig. 6(b) which is near the fan-para transitions.

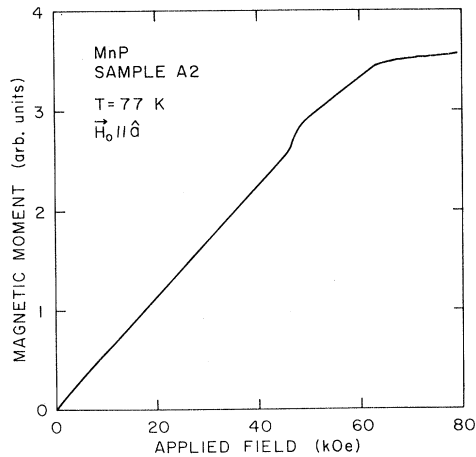


FIG. 8. Trace of the magnetization vs applied magnetic field at 77 K.

fan transition field H_{0f} was taken at the maximum of the sharp susceptibility spike, as before. For the fan-para transition field $H_{0\lambda}^*$ two choices were made: Either at the maximum of the peak (indicated by arrow 1 in Fig. 11), or at the intersection of the two tangents drawn at the inflection points (arrow 2 in Fig. 11). The difference between these two choices was quite small, amounting to no more than ~ 0.1 kOe. For reasons which will be discussed later, we prefer the first choice for $H_{0\lambda}^*$ (at the maximum of the peak) over the second. Figure 12 shows the phase diagram for sample A1 obtained with this choice for $H_{0\lambda}^*$ and a similar choice for the ferro-para transition field $H_{0\lambda}$. The temperatures for this set of data are accurate to better than 0.05 K. Estimates of the demagnetization corrections indicate that the internal fields at the various transitions are 1% lower than the applied fields shown in Fig. 12.

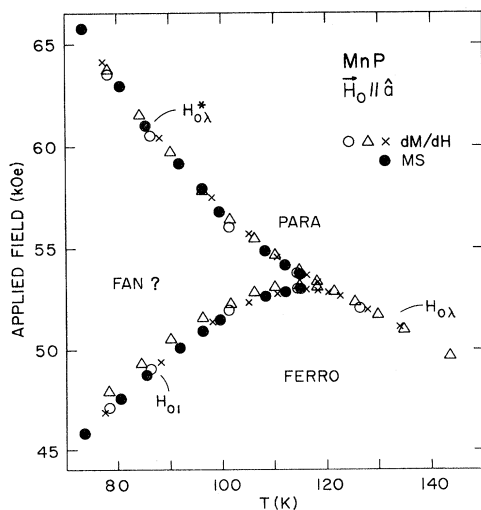


FIG. 9. Phase diagram near the PFF triple point. Data are for sample A2.

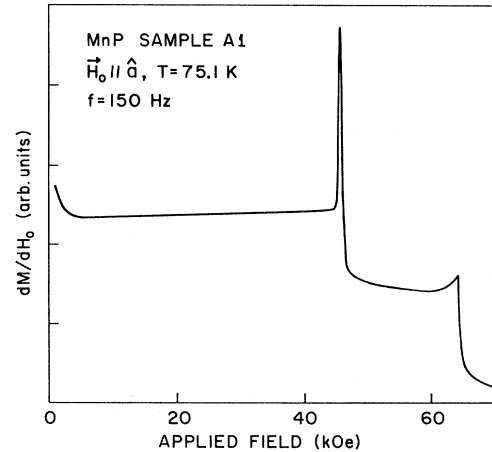


FIG. 10. Trace of dM/dH_0 for sample A1 as a function of applied field H_0 . Sharp spike and the λ anomaly correspond to the ferro-fan and fan-para transitions, respectively.

VI. PARA-FERRO-FAN TRIPLE POINT

A. Qualitative features which agree with a LP

The para, ferro, and fan (PFF) phases meet at the PFF triple point, located at $T = T_t$ and $H_0 = H_{0t}$. The corresponding internal magnetic field is H_t . From the results for sample A2 (Fig. 9) it is estimated that $T_t = 123 \pm 3$ K and $H_{0t} = 53$ kOe. Using the latter value and the demagnetization correction, we obtain $H_t = 51$ kOe. From fits of the more accurate data for sample A1 (discussed later) we obtain $T_t = 120.7 \pm 0.4$ K. For this sample $H_{0t} = 51.5$ kOe and $H_t = 51$ kOe.

Assuming that the magnetic structure of the fan phase is indeed that of a fan, the PFF triple point is a meeting point of a disordered phase (para), an ordered phase with a uniform magnetization (ferro), and a modulated phase (fan). This is one of the basic requirements for the Lifshitz point introduced by Hornreich *et al.*¹⁵ Thus, it is

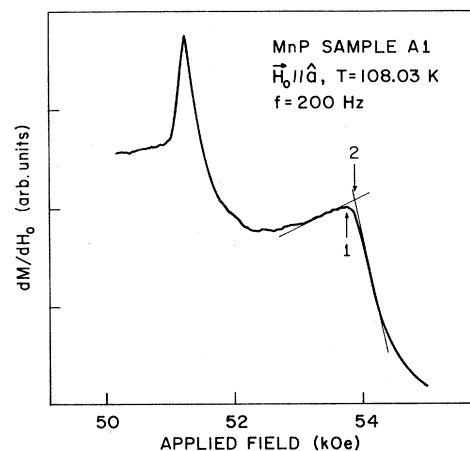


FIG. 11. Trace of dM/dH_0 vs H_0 for sample A1. Two arrows, marked by 1 and 2, indicate two choices for the fan-para transition field.

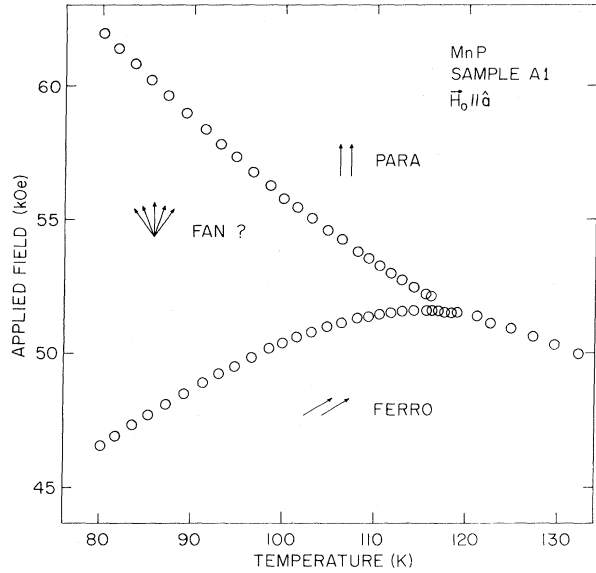


FIG. 12. Phase diagram near the PFF triple point. Data are for sample A1.

possible that the PFF triple point in the configuration $\vec{H}||a$ is a LP. Some support for this conjecture is given by the striking similarity of the phase diagram near this PFF triple point (Figs. 2, 9, and 12) and that near the PFF triple point in the configuration $\vec{H}||b$ (Fig. 1). There is a strong evidence that the latter triple point is a LP.²⁻⁷

If the PFF triple point for $\vec{H}||a$ is a LP, then it should belong to the universality class $d=3, n=m=1$. Here, d and n are the lattice and spin dimensionalities, respectively, and m is the number of components of \vec{q} in the modulated phase. The reasons for this assignment are the ferro-para transition is Ising-like ($n=1$), and \vec{q} in the fan phase is expected to be parallel to a ($m=1$).

The phase boundaries for a LP with $d=3, n=m=1$ were calculated by several authors.^{18,19,29,30} From these calculations one expects that all the phase boundaries will be tangent to each other at the LP, and that the λ line (separating the para phase from the ordered phases) will have an inflection point at the LP. Also, from a Landau-type calculation²⁹ one expects the ferro-fan transition to be of first order. The PFF triple point for $\vec{H}||a$ has all these features.

B. Crossover exponent

The analysis of the phase boundaries near the PFF triple point follows closely the procedure described in Ref. 3. Briefly, we assume that the PFF triple point is a multicritical point which obeys generalized scaling. Under this assumption the shapes of the phase boundaries near (T_i, H_i) should be governed by a crossover exponent ϕ . To obtain ϕ , two scaling axes in the T - H plane are introduced. One axis is tangent to the phase boundaries at the multicritical point. The other axis is chosen to be parallel to the H axis. From the scaling assumption it then follows that near the multicritical point,

$$H_\lambda^* - H_1 = A(T_i - T)^{1/\phi}, \quad (2)$$

where H_λ^* and H_1 are measured at the same T , and A is a constant. The derivation of Eq. (2) does not require the multicritical point to be a LP.

In comparing the data with Eq. (2) we used the applied fields $H_{0\lambda}^*$ and H_{01} rather than the internal fields H_λ^* and H_1 . This is justified later. The data which were compared with Eq. (2) were obtained with sample A1. (These are more accurate than those for sample A2.) We used two sets of such data. The first, shown in Fig. 12, was based on the choice of $H_{0\lambda}^*$ at the maximum of the differential susceptibility. This is choice 1 in Fig. 11. The second set of data was based on choice 2 in Fig. 11. The first set of data included pairs of $H_{0\lambda}^*$ and H_{01} at temperatures up to $T_f = 116.2$ K, which was the highest temperature at which the susceptibility peak at the fan-para transition was resolved. For the second set of data the highest temperature was $T_f = 118.9$ K. It is noteworthy that although the two choices for $H_{0\lambda}^*$ always differed by less than ~ 0.1 kOe, this difference was not always negligible compared to $H_{0\lambda}^* - H_{01}$. Thus the difference between the two values for $H_{0\lambda}^*$ was 2% of $H_{0\lambda}^* - H_{01}$ at 99.9 K, 6% at 110.5 K, and 19% at 115.5 K.

Several least-squares fits were made for each of the two sets of data. In any particular fit, only data points in the range $T_i \leq T \leq T_f$ were included. The initial temperature T_i varied from fit to fit, but the final temperature T_f was kept fixed (i.e., 116.2 K for the first set of data and 118.9 K for the second). The purpose of this procedure was to obtain the dependence of the fitting parameters ϕ , T_i , and A on the range of the fit. Figure 13 shows the results for

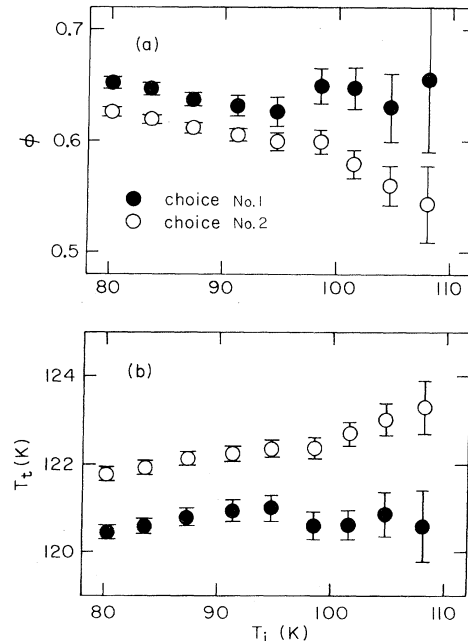


FIG. 13. Results for the temperature T_i of the PFF triple point, and for the crossover exponent ϕ , as obtained from fits of the data for sample A1 to Eq. (2). The temperature T_i specifies the range which is covered in a particular fit (see text). Solid and empty circles correspond to two choices for the fan-para transition field (see Fig. 11).

ϕ and T_t obtained with several T_t 's between 80 and 110 K. For the set of data which was based on choice 1 (i.e., $H_{0\lambda}^*$ at the maximum of the differential susceptibility) the values of ϕ and T_t do not show a strong systematic dependence on the range of the fit. However, for the second set of data, ϕ decreases and T_t increases when the initial temperature of the fit is increased. For this reason we regard choice 1 as more satisfactory. This choice is also consistent with the usual criterion for a second-order magnetic transition when the differential susceptibility peak is sharp. The reason that choice 2 was also used in the present work is the following. When the peak in $\partial M/\partial H_0$ is rounded, or is very small, it is difficult to determine the transition field accurately. Under such circumstances, one practical method of obtaining an estimate for the transition field is to use choice 2.

Based on the results in Fig. 13 for choice 1, we estimate that $\phi=0.64\pm 0.02$ and $T_t=120.7\pm 0.4$ K. Mean-field theory for the LP gives $\phi=0.5$, which is lower than our experimental result. However, a calculation to first order in ϵ for a LP with $d=3, n=m=1$, gives $\phi=0.625$ (Ref. 30), which is in agreement with our result for ϕ . The value of T_t is identical, within the experimental accuracy, with the temperature of the PFF triple point for $\vec{H}||b$.³

We now consider the errors caused by the replacement of the internal magnetic fields in Eq. (2) by the applied fields at the transitions. The demagnetization correction for $H_{0\lambda}^* - H_{01}$ depends on the average susceptibility $\Delta M/\Delta H$ between the middle of the ferro-fan transition and the fan-para transition. On the basis of Figs. 8, 10, and 11 we expect that for a given T this average susceptibility is lower than the low- H susceptibility. The low- H susceptibility in this temperature range is $\sim 8 \times 10^{-3}$ emu/cm³ (Ref. 13). Using $N_a \simeq 1$ for sample A1, we therefore estimate that the difference between $H_{0\lambda}^* - H_{01}$ and $H_{\lambda}^* - H_1$ is less than 1%. This small difference, however, may vary slightly between 80 and 120 K, and this variation can affect the results for ϕ and T_t . To get a rough upper bound for the magnitude of these errors we followed a procedure designed to grossly overestimate the variation of the demagnetization correction. We assumed that the difference between $H_{0\lambda}^* - H_{01}$ and $H_{\lambda}^* - H_1$ changed between 0% at 120 K and 1% at 80 K, with a linear dependence on T between these two temperatures. The least-squares fits were then rerun with this demagnetization correction using T_t 's between 80 and 110 K. Here, the set of data corresponding to choice 1 was used. The results for T_t did not differ by more than 0.06 K from the corresponding results without the assumed demagnetization correction. The difference in the values for ϕ was always less than 0.004. We therefore conclude that the neglect of the demagnetization correction had an insignificant effect on the results of the least-squares fits.

C. Discussion

The evidence that the PFF triple point for $\vec{H}||a$ is a LP can be summarized as follows. (1) The phase diagram near this point is similar to that near the corresponding point for $\vec{H}||b$. The evidence that the latter point is a LP is quite strong.²⁻⁷ (2) There is a close agreement between

the temperatures of the PFF triple points for $\vec{H}||a$ and $\vec{H}||b$, which suggests, again, that the character of the two multicritical points is the same. (3) The qualitative shapes of the phase boundaries agree with predictions for a LP. (4) The crossover exponent ϕ is consistent with a LP. On the other hand, neutron scattering data, which are crucial for establishing the Lifshitz character of the multicritical point, are still missing for the configuration $\vec{H}||a$. Thus, there is no definitive evidence that the structure of the fan phase for $\vec{H}||a$ is indeed that of a fan. In addition, there are no data which show that the propagation vector \vec{q} in this fan phase goes continuously to zero as the PFF point is approached, which is required for a LP. Until such data become available, the conclusion that the PFF triple point for $\vec{H}||a$ is a LP should be regarded as very plausible but still tentative.

The PFF triple points in the configurations $\vec{H}||a$ and $\vec{H}||b$ occur at very different values of the magnetic field, but at the same temperature (120.7 ± 0.4 and 121 ± 1 K). The factor-of-3 difference in the values of the magnetic field at these points is related to the different anisotropies for the a and b directions. The agreement of the two temperatures can be explained in a natural way if one assumes that both points are LP's and that the effective exchange constants of MnP depend on T but are independent of the direction and magnitude of \vec{H} . As mentioned in Sec. I, competing exchange interactions can lead to a LP if the ratios of the exchange constants satisfy certain requirements. In the simplest case of two exchange constants, the ratio $\kappa=J_2/J_1$ should be equal to κ_L .^{18,19} A mean-field treatment of the more general case shows that the Fourier transform $J(\vec{k})$ of the exchange interactions should have certain properties at the LP (see, e.g., Ref. 5). Thus, if the effective exchange constants of MnP depend only on T then the condition for the occurrence of a LP will be met at the same temperature for both $\vec{H}||a$ and $\vec{H}||b$. The situation for the configuration $\vec{H}||c$ is completely different because the c component of \vec{H} is the ordering field for the ferro phase.³ Finally we remark that the observed H dependence of q in the fan phase, when \vec{H} is parallel to b ,^{4,14} does not imply that the exchange constants depend on H . The H dependence of q for fixed exchange constants was discussed theoretically by Enz³¹ and by Nagamiya.³²

VII. BOUNDARIES OF THE CONE PHASE

The cone phase is surrounded by two boundaries: cone-ferro and cone-fan. The cone-ferro boundary is a line of first-order transitions. The low- H portion of this boundary was determined from TE measurements at various fixed values of H_0 . The high- H portion of the boundary was obtained from traces of the MS at various fixed T 's. These measurements were performed on samples A2 and B. Figure 14 shows an example of the MS data. In this example the magnitude of the change in the length at the transition is $\delta l/l \sim 10^{-5}$. The results for the cone-ferro phase boundary, and portions of the cone-fan and ferro-fan phase boundaries, are shown in Fig. 15. The applied magnetic field in this figure is approximately 3.5%

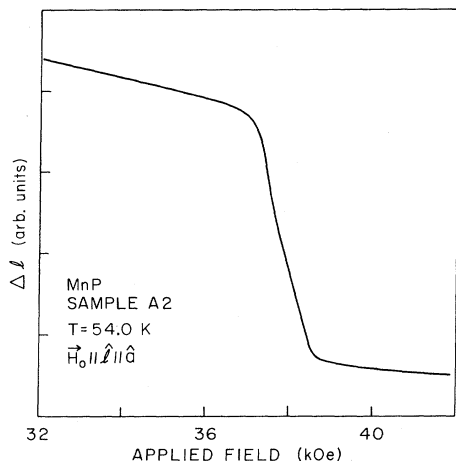


FIG. 14. Trace of the longitudinal MS near the ferro-cone transition at 54.0 K.

higher than the internal field H .

The transition between the cone and fan phases was investigated by the differential susceptibility and MS techniques. It was also observed in magnetization measurements at 4.2 K. Figure 16 shows an example of the latter data as well as the magnetization curves for the other two principal crystallographic directions of MnP. For $\vec{H} \parallel a$ the magnetization curve in Fig. 16 indicates the existence of two transitions: cone-fan at $H_0 \approx 59$ kOe and fan-para at $H_0 \approx 87$ kOe (near the top of the trace). Both transitions appear to be of second order. The magnetization curves for $\vec{H} \parallel b$ and $\vec{H} \parallel c$ show the transitions mentioned in Sec. I, which were studied in earlier works.^{3,9,13} Note that the saturation moment for all three directions is the same within the experimental accuracy. Its value is 84.3 ± 2 emu/g, which corresponds to 1.30 ± 0.03 Bohr magnetons per Mn atom.

Differential susceptibility data on sample A2 were consistent with the interpretation that the cone-fan transition at 4.2 K is of second order. However, the data at much

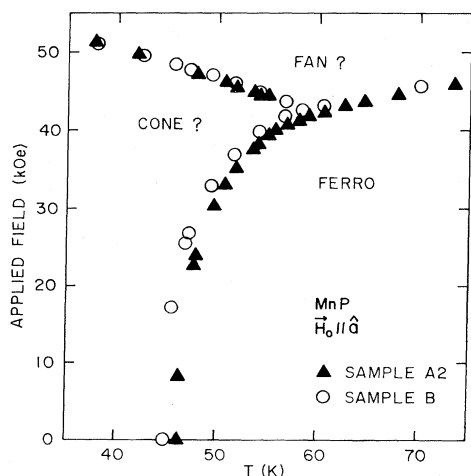


FIG. 15. Phase boundaries near the cone-ferro-fan triple point as obtained from MS and TE data on samples A2 and B.

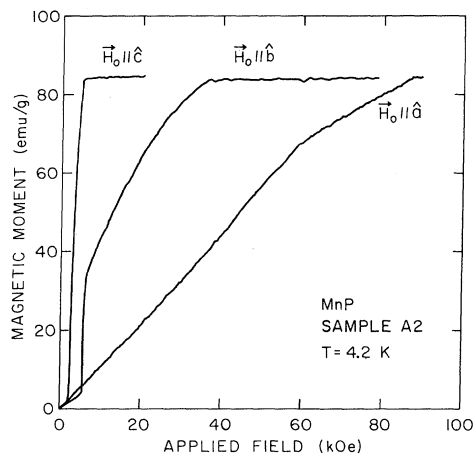


FIG. 16. Traces of the magnetization vs H_0 at 4.2 K for fields applied parallel to the three principal crystallographic directions.

higher temperatures did not give a clear indication of the order of the transition. This uncertainty was not removed by MS data which were taken on samples A2 and B. That is, we were unable to determine whether there were small discontinuities in the magnetization M and the sample's length l at the transition.

To resolve this difficulty a more detailed study of the ac differential susceptibility was performed on sample A1, with \vec{H}_0 aligned to within 0.1° from the a axis. In this study the out-of-phase (quadrature) component of the signal was measured in addition to the in-phase component. The quadrature component (which is sensitive to losses) is expected to exhibit a sharp spike at a first-order transition, but not at a second-order transition. The reason is the following. At a first-order transition, domains of two dissimilar phases coexist. The ac modulation field causes a motion of the domain walls. This motion is associated with energy dissipation. Because this loss mechanism occurs only in the narrow field interval in which the domains coexist, the quadrature component versus H_0 should have a sharp spike at the transition. At a second-order transition the two phases are identical, and there are no domains. Therefore, energy dissipation due to domain-wall motion does not occur. These expectations for the different behaviors of the quadrature component at first- and second-order transitions were confirmed in measurements near the ferro-fan and fan-para transitions. The setup which was used to study the cone-fan transition was the same.

Examples of the ac susceptibility data at several temperatures are shown in Fig. 17. These data were taken at a frequency $f = 45$ Hz and a modulation amplitude of ~ 0.5 Oe. For this frequency the estimated skin depth at $T = 4$ K is 1.4 cm, which is 28 times the sample's thickness. [This is based on the resistivity ratio $\rho(273 \text{ K})/\rho(4 \text{ K}) = 67$ for this crystal,³ and the known room-temperature resistivity.¹¹] At higher temperatures the skin depth should be larger. Thus the phase of the oscillating magnetic field inside the sample should be very nearly the same as that of the applied modulation field. All the curves in Fig. 17 (both for the in-phase and the quadrature

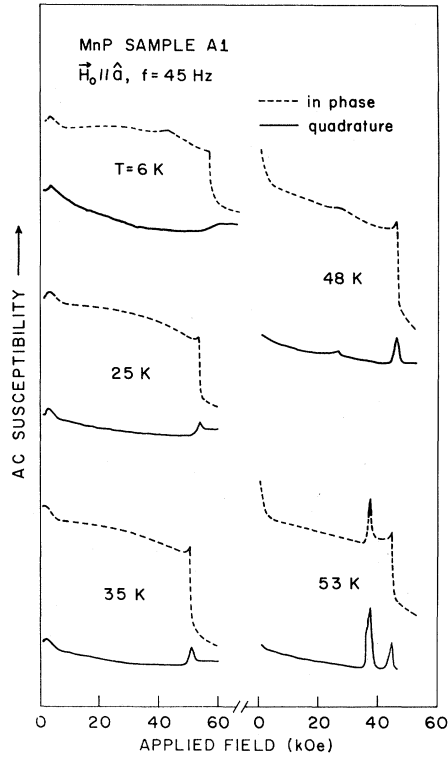


FIG. 17. Recorder traces of the in-phase and quadrature components of the ac susceptibility of sample A1 at various temperatures. All traces were obtained with the same gain.

components) were obtained with the same gain.

At 6 K the in-phase component shows a rapid decrease near the cone-fan transition at $H_0 = 58$ kOe. The quadrature component also shows a small change, but it does not exhibit a spike. The reason for the change in the quadrature component is not known. (It might have been caused by a small error in the phase setting of the lock-in amplifier used to detect the imbalance signal of the ac bridge. No change in the quadrature component at the cone-fan transition was observed at 200 Hz.) It is noteworthy that the in-phase component at 6 K exhibits some structure below the cone-fan transition. It consists of a well-defined peak near 4 kOe and two small broad peaks at higher fields. The peak at 4 kOe will be discussed in Sec. VIII. The origin of the remaining structure is unclear, but its existence suggests that the evolution of the cone phase with increasing H_0 may involve several broad stages. Measurements with higher modulation frequencies, at $T = 6$ K, confirmed the existence of the structure in the in-phase component below the cone-fan transition.

At 25 K the in-phase component does not exhibit a distinct structure below the cone-fan transition, except for the peak at low H_0 which will be discussed later. At the cone-fan transition the in-phase component has a small peak which is followed by a rapid decrease. The small peak may be interpreted in two ways. (1) It is a peak associated with a second-order transition. It arises because the critical fluctuations at 25 K are stronger than at 6 K. (2) It is a small spike associated with a small discontinuity in the magnetization, in which case the transition is weakly

first order. The existence of a small peak in the quadrature component suggests that the latter interpretation is correct. At 35 K the situation is similar except that the peaks in both the in-phase and quadrature components are slightly larger.

The traces at 48 K show that the peaks in the in-phase and quadrature components at the cone-fan transition continue to grow. The additional small peak (in both components) near 27 kOe is due to the ferro-cone transition which now appears because the temperature is higher than T_a . Note that at 48 K the quadrature peak at the cone-fan transition is larger than the peak in the in-phase component. (The vertical scale for both components is the same.) Thus, the peak in the quadrature component cannot be attributed to a small error in the setting of the phase of the lock-in amplifier. Note also that the quadrature signal is nearly constant at fields just above the peak, whereas the in-phase component decreases rapidly. This indicates that the error in the phase setting, if any, is small. The traces at 53 K show similar features at the cone-fan transition, but the peaks at the ferro-cone transition (near 38 kOe) are much larger than at 48 K. The last feature is probably due to the fact that the ferro-cone phase boundary is more nearly parallel to the T axis at 53 K than at 48 K (see Fig. 15). This makes the transition at 53 K (observed at a fixed T) sharper than at 48 K.

The peak in the quadrature component at the cone-fan transition was observed at all temperatures above about 15 K. This suggests that at these temperatures the transition is of first order. Further evidence for this conclusion comes from the frequency dependence of the peaks for the in-phase and quadrature component. The frequency dependence was studied in the range $45 \leq f \leq 2000$ Hz using roughly the same modulation amplitude (~ 0.5 Oe). The results showed that both the in-phase and quadrature peaks at the cone-fan transitions above ~ 15 K decreased rapidly in magnitude as f increased. (This statement refers to the peaks in χ' and χ'' , i.e., the usual dependence of the output on frequency and modulation amplitude was corrected for.) A similar decrease of the peaks with increasing f was also observed at the ferro-cone and ferro-fan transitions, which are of first order. In contrast, the λ peak for the in-phase component at the fan-para transition (second order) did not show an appreciable dependence on frequency. The same insensitivity of the in-phase signal to frequency was observed generally, except for the peaks at the first-order transitions. The frequency dependence at the first-order transitions probably arose because the domain walls were unable to follow the ac modulation field when the frequency became high.

On the basis of the preceding data we believe that the cone-fan transitions above approximately 15 K are weakly first order. Well below 15 K the transitions are either of second order (in which case there exists a tricritical point on the cone-fan boundary) or are very weakly first order.

VIII. LOW-FIELD ANOMALY

In this section we discuss some observations which appear to be due to sample imperfections.

Figure 17 shows that the ac susceptibility of sample A1

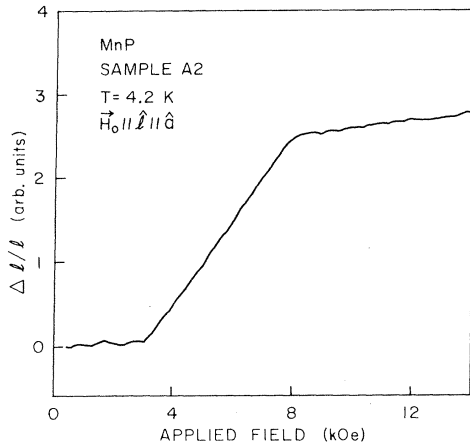


FIG. 18. MS of sample A2 at 4.2 K showing the low-field anomaly.

exhibits an anomaly in fields of several kOe. For $T < T_\alpha = 46$ K the anomaly appears as a peak in both the in-phase and quadrature components. This resembles a first-order transition. Above T_α the in-phase component decreases rapidly between $H_0 = 0$ and $H_0 \approx 5$ kOe. The latter behavior is also seen in Fig. 10.

An extensive study of the low-field anomaly was made using the MS technique. Samples A2 and B were used. Below T_α , the anomaly appeared as a jump $\delta l/l$ in the length of the sample. An example is shown in Fig. 18. This behavior resembled a first-order transition. However, several observations indicated that this "transition" was not an intrinsic property of MnP in the configuration $\vec{H} \parallel a$. First, the magnitude of the jump $\delta l/l$ in sample B was an order of magnitude smaller than that in sample A2. For example, at 4.2 K, $\delta l/l = 4 \times 10^{-6}$ for sample A2, but only 0.5×10^{-6} for sample B. This sample dependence should be contrasted with the behavior near the cone-ferro and ferro-fan transitions for which $\delta l/l$ was the same for both samples. Another feature of the low-field anomaly which is inconsistent with an intrinsic transition is the large width of the anomaly in Fig. 18, $\Delta H_0 \approx 5$ kOe. If one equates this width to $N_a \Delta M$, where ΔM is the jump in the magnetization and $N_a \approx 5$, one obtains a value for ΔM which is twice the saturation magnetization of MnP. This, of course, is impossible. A close examination of the magnetization curve of sample A2 at 4.2 K shows that ΔM is, in fact, only $\sim 1\%$ of the saturation magnetization. Finally we note that the low-field anomaly in the ac susceptibility (Fig. 17) persists at temperatures above T_α , where the magnetic order is ferromagnetic and no low-field anomaly is expected when \vec{H} is parallel to the hard direction.

An explanation of the low-field anomaly can be given on the basis of the following assumptions. (1) Each of our samples contained small crystallites which were misoriented relative to the bulk of the sample. These misoriented crystallites will be referred to as MCR's. (2) The c axis for a substantial portion of the MCR's was within 60° or so from the a axis of the main portion of the sample. (3) The volume fraction occupied by the MCR's was of order

1% for samples A1 and A2, but was an order of magnitude smaller for sample B.

It is known that below T_α , a screw-ferro transition occurs at low fields when \vec{H} is parallel to the c axis (see, e.g., Fig. 16). This transition also occurs when \vec{H} makes a finite angle θ with the c axis. For $0^\circ \leq \theta \leq 60^\circ$ and $T \ll T_\alpha$, the internal magnetic field at the transition is in the range 2–4 kOe (see Fig. 9 of Ref. 10). We attribute the low-field anomaly below T_α to a screw-ferro transition in the MCR's. This explanation is supported by the following facts. (i) The magnitude and temperature dependence of the applied field at which the low-field anomaly starts agree with the known properties of the screw-ferro transition for small θ 's. (ii) For a given sample the width ΔH_0 of the low-field anomaly is independent of T below T_α . This is expected for a fixed distribution of MCR's, each with a fixed demagnetizing factor N , because the jump ΔM at the screw-ferro transition is nearly independent of T . (For small θ 's, ΔM is approximately equal to the saturation magnetization of MnP.) We also note that the width $\Delta H_0 \approx 5$ kOe for sample A2 is consistent with either a single MCR for which $N \approx 10$, or with a distribution of MCR's with various θ 's and N 's. The width ΔH_0 in sample B was smaller than in sample A2. (iii) Measurements of the MS near the screw-ferro transition at 4.2 K, performed with \vec{H} parallel to the c axis, showed a pattern which was very similar to that in Fig. 18. The main difference was that the jump $\delta l/l = 80 \times 10^{-6}$ was much larger than in Fig. 18. This is expected because the signal in Fig. 18 arises from only a small portion of the sample, whereas for $\vec{H} \parallel c$ the signal involves the bulk of the sample.

The assumption that MCR's exist in our samples also leads to a natural explanation of the low-field behavior of the ac susceptibility above T_α (Figs. 10 and 17). When a magnetic field is applied it aligns the ferromagnetic moment of the MCR's, because in each MCR there is a substantial field component along the easy-magnetization axis. Once the moments in the MCR's become aligned, the ac susceptibility drops. This occurs at a field of several kOe.

It must be emphasized that the low-field anomalies associated with the MCR's did not affect the results for the phase transitions which were intrinsic to the configuration $\vec{H} \parallel a$. The intrinsic phase transition occurred at much higher fields, and were sample independent. The results of our previous work, for the configuration $\vec{H} \parallel b$,³ also were not affected by the MCR's. The MCR's were not detected in our previous work.

IX. SUGGESTIONS FOR FURTHER STUDIES

The present work is only a step toward understanding the magnetic phases and magnetic transitions of MnP in the configuration $\vec{H} \parallel a$. Further studies are necessary to clarify several remaining problems. (1) The structures of the fan and cone phases are still to be confirmed by neutron scattering techniques. (2) The variation of the propagation vector \vec{q} in the fan phase and in the cone phase should be studied using neutron diffraction. In particular,

it is important to determine whether, in the fan phase, q approaches zero continuously as the PFF triple point is approached. This property is an essential feature of a LP. Assuming that q does go continuously to zero, the exponent β_k which governs the approach to zero on the fan-para boundary should be measured and compared with predictions for the LP.^{4,16,33} (3) More detailed studies of the cone-fan transition are necessary in order to determine the order of the transition at low temperatures. (4) The low-field anomaly should be studied in different MnP crystals. If our explanation of the anomaly is correct then the anomaly should not be observed in crystals of the highest quality. (5) Theoretical calculations concerning the cone structure in MnP, and the cone-fan transition, are needed. A mean-field calculation for the

Hiyamizu-Nagamiya model¹⁰ (or for a simplified version of this model⁷) will be an important first step in this direction.

ACKNOWLEDGMENTS

We wish to thank Dr. B. Golding for kindly providing one of the samples. The Francis Bitter National Magnet Laboratory is supported by the National Science Foundation. The Instituto de Física, Universidade de São Paulo is supported by Financiadora de Estudos e Projetos (FINEP). This work was supported in part by a joint grant from the U. S. National Science Foundation and the Brazilian Conselho Nacional de Desenvolvimento Científico e Tecnológico (CNPq).

- ¹An extensive list of references for experimental works on MnP is given in Ref. 3.
- ²C. C. Becerra, Y. Shapira, N. F. Oliveira, Jr., and T. S. Chang, *Phys. Rev. Lett.* **44**, 1692 (1980).
- ³Y. Shapira, C. C. Becerra, N. F. Oliveira, Jr., and T. S. Chang, *Phys. Rev. B* **24**, 2780 (1981).
- ⁴R. M. Moon, J. W. Cable, and Y. Shapira, *J. Appl. Phys.* **52**, 2025 (1981).
- ⁵C. S. O. Yokoi, M. D. Coutinho-Filho, and S. R. Salinas, *Phys. Rev. B* **24**, 5430 (1981).
- ⁶Y. Shapira, *J. Appl. Phys.* **53**, 1914 (1982).
- ⁷Y. Shapira, in *Proceedings of the NATO Advanced Study Institute on Multicritical Phenomena*, Geilo, Norway, 1983 (to be published).
- ⁸Y. Shapira and N. F. Oliveira, Jr., *Phys. Lett.* **89A**, 205 (1982).
- ⁹T. Komatsubara, T. Suzuki, and E. Hirahara, *J. Phys. Soc. Jpn.* **28**, 317 (1970).
- ¹⁰S. Hiyamizu and T. Nagamiya, *Int. J. Magn.* **2**, 33 (1972).
- ¹¹A. Takase and T. Kasuya, *J. Phys. Soc. Jpn.* **48**, 430 (1980).
- ¹²G. P. Felcher, *J. Appl. Phys.* **37**, 1056 (1966); J. B. Forsyth, S. J. Pickart, and P. J. Brown, *Proc. Phys. Soc. London* **88**, 333 (1966); H. Obara, Y. Endoh, Y. Ishikawa, and T. Komatsubara, *J. Phys. Soc. Jpn.* **49**, 928 (1980); R. M. Moon, *J. Appl. Phys.* **53**, 1956 (1982).
- ¹³E. E. Huber, Jr. and D. H. Ridgley, *Phys. Rev.* **135**, A1033 (1964).
- ¹⁴Y. Ishikawa, T. Komatsubara, and E. Hirahara, *Phys. Rev. Lett.* **23**, 532 (1969).
- ¹⁵R. M. Hornreich, M. Luban, and S. Shtrikman, *Phys. Rev. Lett.* **35**, 1678 (1975).
- ¹⁶R. M. Hornreich, *J. Magn. Magn. Mater.* **15-18**, 387 (1980).
- ¹⁷K. Tajima, Y. Ishikawa, and H. Obara, *J. Magn. Magn. Mater.* **15-18**, 373 (1980).
- ¹⁸S. Redner and H. E. Stanley, *Phys. Rev. B* **16**, 4901 (1977); *J. Phys. C* **10**, 4765 (1977).
- ¹⁹W. Selke, *Z. Phys. B* **29**, 133 (1978); W. Selke and M. E. Fisher, *Phys. Rev. B* **20**, 257 (1979); *J. Magn. Magn. Mater.* **15-18**, 403 (1980).
- ²⁰E. Maxwell, *Rev. Sci. Instrum.* **36**, 553 (1965).
- ²¹After the susceptibility data on sample A2 were taken, a small piece of the sample broke off. The MS data were taken on the remaining sample, for which the estimated demagnetizing factor was slightly smaller than the original. In plots of the MS results for the phase diagram, the values of H_0 were adjusted to correspond to the original demagnetizing factor. This adjustment was typically 0.7%. No such adjustment was made in figures which show traces of the MS as a function of H_0 .
- ²²N. F. Oliveira, Jr., A. Paduan Filho, S. R. Salinas, and C. C. Becerra, *Phys. Rev. B* **18**, 6165 (1978).
- ²³Y. Kitano and T. Nagamiya, *Prog. Theor. Phys.* **31**, 1 (1964). See, in particular, Sec. 4 and Fig. 8.
- ²⁴In the limit $H \rightarrow 0$ the cone becomes a spiral. Recent experiments show that this spiral is circular, but the spins are bunched up near the $\pm c$ directions (see R. M. Moon in Ref. 12). From the work of Kitano and Nagamiya we expect that at finite H the cone is elliptical. However, some bunching up of the spins may also occur in the cone phase. That is, the projections of the spins on the b - c plane may be more crowded near the $\pm c$ directions.
- ²⁵H. Terui, T. Komatsubara, and E. Hirahara, *J. Phys. Soc. Jpn.* **38**, 383 (1975).
- ²⁶H. Thomas, *Phys. Rev.* **187**, 630 (1969).
- ²⁷E. Riedel and F. Wegner, *Z. Phys.* **225**, 195 (1969).
- ²⁸G. V. Lecomte, M. Karnezos, and S. A. Friedberg, *J. Appl. Phys.* **52**, 1935 (1981).
- ²⁹A. Michelson, *Phys. Rev. B* **16**, 577 (1977).
- ³⁰D. Mukamel and M. Luban, *Phys. Rev. B* **18**, 3631 (1978).
- ³¹U. Enz, *J. Appl. Phys.* **32**, 22S (1961).
- ³²T. Nagamiya, *J. Appl. Phys.* **33**, 1029 (1962).
- ³³D. Mukamel, *J. Phys. A* **10**, L249 (1977).